TITLE: Serial block-face scanning electron microscopy applied to study the trafficking of 8D3-coated gold nanoparticles at the blood-brain barrier

AUTHORS: Itsaso Cabezón[†,‡,§] , Elisabet Augé,[†,§], Manel Bosch[ǁ], Alison J. Beckett[#], Ian A. Prior[#], Carme Pelegrí,[†,§,¶,⊥], Jordi Vilaplana[*,†,§,¶,⊥]

[⊥] These authors contributed equally to this study

AFFILIATIONS:

[†]Secció de Fisiologia, Departament de Bioquímica i Fisiologia, Facultat de Farmàcia i Ciències de l'Alimentació, Universitat de Barcelona, Barcelona, Spain

[‡]Unitat de Farmacologia i Farmacognòsia, Facultat de Farmàcia i Ciències de l'Alimentació, Universitat de Barcelona, Barcelona, Spain

[§]Institut de Neurociències, Universitat de Barcelona, Barcelona, Spain

[ǁ]Unitat de Microscòpia Òptica Avançada, Centres Científics i Tecnològics de la Universitat de Barcelona (CCiTUB), Barcelona, Spain

[#]Division of Cellular and Molecular Physiology, Institute of Translational Medicine, University of Liverpool

[¶]CIBERNED Centros de Biomedicina en Red de Enfermedades Neurodegenerativas, Spain

E-MAIL ADDRESSES: itsaso.cabezon@ub.edu; eauge@ub.edu; mbosch@ccit.ub.edu; A.J.Beckett@liverpool.ac.uk; iprior@liverpool.ac.uk; carmepelegri@ub.edu; vilaplana@ub.edu

CORRESPONDING AUTHOR: *Jordi Vilaplana, Secció de Fisiologia, Departament de Bioquímica i Fisiologia, Facultat de Farmàcia i Ciències de l'Alimentació, Universitat de Barcelona, Av. Joan XXIII 27-31, 08028 Barcelona, Spain. Tel. (+34) 93 4024505. E-mail: vilaplana@ub.edu

1

ABSTRACT

Due to the physical and physiological properties of the blood-brain barrier (BBB), the transport of neurotherapeutics from blood to brain is still a pharmaceutical challenge. We previously conducted a series of experiments to explore the potential of the anti-transferrin receptor 8D3 monoclonal antibody (mAb) to transport neurotherapeutics across the BBB. In that study, gold nanoparticles (AuNPs) were coated with the 8D3 antibody and administered intravenously to mice. Transmission electron microscopy was used and a two-dimensional (2D) image analysis was performed to detect the AuNPs in the brain capillary endothelial cells (BCECs) and brain parenchyma. In the present work, we determined that serial block-face scanning electron microscopy (SBF-SEM) is a useful tool to study the transcytosis of these AuNPs across the BBB in three dimensions and we therefore applied it to gain more knowledge of their transcellular trafficking. The resulting 3D reconstructions provided additional information on the endocytic vesicles containing AuNPs and the endosomal processing that occurs inside BCECs. The passage from 2D to 3D analysis reinforced the trafficking model proposed in the 2D study, and revealed that the vesicles containing AuNPs are significantly larger and more complex than described in our 2D study. We also discuss tradeoffs of using this technique for our application, and conclude that together with other volume electron microscopy imaging techniques, SBF-SEM is a powerful approach that is worth of considering for studies of drug transport across the BBB.

KEYWORDS: blood-brain barrier, receptor-mediated transport, transferrin receptor, monoclonal antibodies, SBF-SEM, 3D electron microscopy, drug delivery

ABBREVIATIONS: BBB, blood-brain barrier; TfR, transferrin receptor; mAb, monoclonal antibody; AuNP, gold nanoparticle; TEM, transmission electron microscopy; 2D, two-dimensional; 3D, three-dimensional; SBF-SEM, serial block-face scanning electron microscopy; BCEC, brain capillary endothelial cell; PBS, phosphate-buffered saline; PF, p-formaldehyde.

INTRODUCTION

The blood–brain barrier (BBB) is a well-coordinated and highly selective barrier that severely limits brain uptake and hence the therapeutic potential of pharmacologically active compounds following intravenous administration (Abbott et al. 2010; de Boer and Gaillard 2007; Pardridge 1998; Temsamani 2001). Receptor-mediated transcytosis in brain capillary endothelial cells (BCECs) has been extensively studied as a possible strategy to transport such compounds across the BBB. Moreover, monoclonal antibodies (mAbs) directed against some of those receptors present in the luminal membrane of BCECs have been proposed as carriers of these substances (Lajoie and Shusta 2015; Manich et al. 2013). Some of these mAbs are those directed against the transferrin receptor (TfR), which have been widely studied in rodents. Some of the studies, principally those using the capillary depletion method or indirect outcome measures to determine brain uptake, conclude that mAbs and/or their cargo are transported across the BBB, while other studies conclude that these mAbs do not complete transcytosis and accumulate inside BCECs (Alata et al. 2014; Gosk et al. 2004; Lee et al. 2000; Manich et al. 2013; Moos and Morgan 2001; Paris-Robidas et al. 2011; Zhang and Pardridge 2005; Zhang et al. 2003). Thus, the success and usefulness of this strategy remain controversial and the intracellular mechanisms by which these mAbs undergo inside or across BCECs are still unknown (Freskgård and Urich 2016). Gaining knowledge of these mechanisms would help to ascertain the possible use of mAbs as molecular Trojan Horses.

We recently conducted a series of experiments to provide insight at a subcellular level into the endocytic/transcytotic mechanisms involved in the processing of these mAbs (Cabezón et al. 2015). In these studies, we coated gold nanoparticles (AuNPs) with the 8D3 antibody directed against the mouse TfR. After *in vivo* administration of the 8D3-AuNP conjugates, and using transmission electron microscopy (TEM), we observed a time-dependent internalization and trafficking pattern (Figure 1). The 8D3-AuNP conjugates were individually internalized within BCECs through clathrin-dependent endocytosis. Thereafter, most of the endocytic vesicles followed an intracellular process of vesicular fusion and rearrangement that ended up moving the AuNPs to late

endosomes, multivesicular bodies or lysosomes, which then presented a high AuNP content. A small percentage of the endocytic vesicles containing just one AuNP followed a different route whereby they fused with the abluminal membrane and opened up to the basal lamina. This latter route suggests endosomal escape and complete transcytosis, but the 8D3 remains attached to the TfR, and thus the 8D3-AuNP conjugates remain in this location, possibly until their reinternalization, without reaching the brain parenchyma beyond the basal lamina.

All these results provided relevant information at an ultrastructural level concerning the dynamics of the AuNP cargo when transported by the possible molecular Trojan Horse 8D3. However, the study was limited by the use of two-dimensional (2D) image analysis. A three-dimensional (3D) structural study could provide significantly more insight into the transport of molecules across the BBB, and more knowledge concerning the trafficking of the AuNPs.

Serial block-face (SBF) imaging is a recently devised approach using scanning electron microscopy (SEM) to acquire serial images and reconstruct large tissue regions in 3D (Ohno et al. 2015). In SBF-SEM, surface areas of the embedded tissue blocks are serially cut and removed with the built-in diamond knife in the SEM chamber between the cycles of SEM imaging. Because the consecutive areas of tissue of the specimens are imaged with surface milling, this method generates largely pre-aligned images, which speeds up 3D reconstruction of the target structures. The method has been extensively used to explore the connectivity of the neuronal network, but only rarely to study the structure of the BBB, and no SBF-SEM data exist on the transport of molecules across this barrier.

The objective of the present work is to determine whether SBF-SEM is a useful tool to study the transcytosis of molecules across the BBB, and their accurate localization both inside BCECs and within other cellular structures of the brain parenchyma. To this end, we coated AuNPs with 8D3 mAb, we administered the resultant 8D3-AuNP conjugates intravenously to mice, and 2.5 hours after administration, we processed the mouse brain for SBF-SEM. We specifically aimed to establish and optimize the configuration

for performing 3D reconstructions of brain regions containing BBB segments and characterize the vesicles containing AuNPs. If the technique is shown to be appropriate, we will complement our previous 2D studies with detailed 3D reconstructions of BBB segments as well as vesicles containing AuNPs situated within BCECs. This will provide additional information regarding these endocytic vesicles and the endosomal processing that occurs inside BCECs.

MATERIALS AND METHODS

Animals

Male ICR-CD1 mice (four months old) were used for the study. They were kept in standard conditions of temperature (22 °C ± 2 °C) and light–dark cycles (12:12 h, 300 lx/0 lx) and had access to food and water *ad libitum* until the day of the experiment. All experimental procedures were reviewed and approved by the University of Barcelona Animal Experimentation Ethics Committee (DAAM 7505).

Formation of the 8D3-AuNP conjugates

8D3–AuNP conjugates were formed as described in Cabezón et al. (2015). Briefly, the anti-TfR 8D3 mAb (AbD Serotec, U.K.) was covalently attached to AuNPs measuring 20 nm in diameter using the InnovaCoat GOLD Covalent Conjugation Kit (Innova Biosciences, Cambridge, U.K.). Then, the buffer was changed to phosphate-buffered saline (PBS), pH 7.2, via four centrifugations of 20 min each at 9000 g, discarding the supernatant and resuspending the pellet in 1200 μL of PBS until the last centrifugation, when the pellet was resuspended in PBS to a final volume of 700 μL.

Administration of the 8D3-AuNP conjugates and brain obtention

The mice were anesthetized with isoflurane, and a bolus of 300 μL of PBS, pH 7.2, containing the 8D3–AuNP conjugate at a concentration of 430 μg of 8D3/mL was intravenously injected into the caudal vein. After 2.5 h of recirculation, the animals were anesthetized with 80 mg/kg of sodium pentobarbital by an intraperitoneal

injection, the thoracic cavity was opened, and an intracardiac gravity-dependent perfusion of 50 mL of PBS followed by 50 mL of paraformaldehyde (PF, Sigma-Aldrich, Madrid, Spain) at 4% and glutaraldehyde at 0.1% in phosphate buffer 0.1 M was performed. The brains were then removed and kept in the same solution.

Brain sample processing for SBF-SEM

Coronal brain sections 1 mm thick were obtained using a vibratome. The hippocampal and cortical areas were then selected, dissected, and post-fixed overnight in PF at 4% and glutaraldehyde at 0.1% in phosphate buffer 0.1 M. The fixative was then substituted for PF at 2%, and tissue samples were stored in this solution for 3 days at 4 °C. Samples were then prepared for SBF-SEM, based on the Deerinck and Ellisman (2010) protocol. The samples were washed in PB 0.1 M and post-fixed with reduced osmium (2% osmium tetroxide (OsO_4) containing 1.5% potassium ferrocyanide) for 1 h at room temperature. Sequentially, the samples were placed in 1% thiocarbohydrazide solution in ddH_2O for 20 min, stained with 2% OsO_4 in ddH_2O for 30 min at room temperature, and incubated in 1% aqueous uranyl acetate (UA) overnight at 4 °C. Between each of the preceding steps, the samples were washed five times, for three minutes each time, with ddH_2O. All the stains were filtered through a 0.22 µm filter, immediately before use.

After overnight incubation, the samples were washed again with ddH_2O five times for three minutes each time, and *en bloc* Walton's lead aspartate staining was performed for 30 min at 60 °C. To prepare the lead aspartate solution, first, 0.399 g of L-aspartic acid (Sigma-Aldrich) was dissolved in 100 ml ddH_2O, and the solution was adjusted to pH 3.8 with 1N KOH. Then, 0.066 g of lead nitrate was dissolved in 10 ml of the aspartic acid stock solution, and the pH was adjusted to 5.5 using 1N KOH.

The tissue was then washed with ddH_2O five times for three minutes each time, and dehydrated through a graded ethanol series (30%, 50%, 70%, and 90%, for 10 min, twice each), followed by 100% propylene oxide (for 10 min twice) at room temperature. The samples were then infiltrated with TAAB Hard Premix resin at ratios

of 1:1, 2:1 and 3:1 with the resin: 100% propylene oxide, 30 mins per incubation. Finally, the samples were incubated in 100% resin for 2 x 30 mins, before embedding in a mold with 100% fresh resin. The samples were cured for 48 h at 60 °C.

Each embedded sample was mounted on an aluminum pin and trimmed to a block face of 0.4 x 0.4 mm^2 using a Leica EM UC6 UltraMicrotome (Leica Microsystems). In order to minimize the charging of the specimen, the samples were silver-painted and sputter-coated (Quorum Technologies, UK) with a thin layer (10 nm) of gold palladium.

Serial block-face scanning electron microscopy

The stained blocks were imaged using a Gatan 3View serial block-face imaging system (Gatan, Pleasanton, CA) installed on a FEI Quanta 250 FEG scanning electron microscope (FEI Company, Hillsboro, OR). The SEM was operated in low vacuum. Image stacks were collected using different setting parameters, depending on the level of magnification. These parameters are detailed in the results section.

Image processing and analysis

The resulting datasets were assembled into volume files and aligned using Digital Micrograph (Gatan UK, Abingdon, UK). 3D reconstruction of the desired structures was performed in image stacks using Imaris 8.0.2 and Imaris 7.2 software (Bitplane). The structures deemed of interest to determine the location of the AuNPs, such as the cellular components of the neurovascular unit (i.e. BCECs, basal membrane, tight junctions, pericytes and astrocytes) and the intracellular endocytic vesicles of the BCECs, among others, were reconstructed in 3D by manually tracing the area in each plane and surface-rendering next. To obtain the 3D representation of the AuNPs, Fiji software (Schindelin et al. 2012) was used following the strategy indicated in the results section.

RESULTS

In an initial attempt to perform a 3D reconstruction of the BBB and to observe the localization of the AuNPs, capillary segments from different brain samples were fully 3D rendered using low-magnification image stacks (10,000-25,000 x). Images were acquired from regions of interest (ROI) of approximately 30,000 nm^3. It must be pointed that the presence of bare resin in the lumen of the capillary, which causes electrical charging of the sample and therefore produces tissue deterioration and even breakage, restricts the possibility of obtaining long series of images. At this level of magnification, we used an incident electron beam with an energy of 2.3-2.4 kV and spot size 3, and a chamber pressure of 50 pa was applied to scan across the samples at a pixel dwell time of 60 µs. As capillaries are not straight and vertical structures, but twisted, and bifurcate within the brain parenchyma, it is difficult to acquire long capillary segments inside the available field of view. However, these conditions permitted us to monitor and acquire images of some transversal capillary segments along the z-axis. These allowed us to identify the cellular elements that form the neurovascular unit and to reconstruct them in 3D. Online Resources 1 and 2 contain the images corresponding to two different stacks obtained at low-magnification. In Online Resource 1, the magnification is 14,900 x and the voxel size is 16 x 16 x 100 nm. Some representative serial images from this stack can be observed in images A1 to C1 in Figure 2. In the same figure, images A2 to C2 indicate the structures selected from A1 to C1 to perform the 3D reconstruction. In this stack, the rendered structures were two adjacent BCECs attached by a tight junction, a pericyte and two different astrocytic endfeet. After the 3D reconstruction, the structures can be visualized from different perspectives, as can be observed in Online Resource 3. Some frames from this video are presented as images D1 to D3 in Figure 2. In Online Resource 2, the magnification is 11,130 x and the voxel size 22.1 x 22.1 x 70 nm. In this case, the rendered structures were a BCEC and a pericyte, and their respective nuclei, and all of them can be visualized from different perspectives on Online Resource 4. Figure 3 shows some images from the stack, some selected structures in these images and some frames from Online Resource 4. Although this level of magnification permits visualization of the neurovascular unit and even the vesicles inside the BCECs (Figure 3,

C1 inset), the AuNPs cannot be clearly visualized: on one hand, due to the low resolution in the x-y plane and on the other hand, due to the backscattered electron signal.

Due to these technical problems, a second attempt with higher magnification imaging of capillary segments was considered to achieve sufficient resolution to visualize the AuNPs. Thus, we acquired higher magnification images (> 30,000 x) from ROIs of approximately 3,000 nm^3. We used an incident electron beam with an energy of 3.5 kV and spot size 3, and a chamber pressure of 50 pa was applied to scan across the samples at a pixel dwell time of 60 μs. At this magnification level, BCECs and the basal membrane of the endothelium can be observed, as well as both the vesicles inside the BCECs and the AuNPs contained in them. Figure 4 is an example of these images: A1-A6 are selected serial images from an SBF-SEM high-magnification image stack (35,850 x; voxel size is 4.8 x 4.8 x 100 nm). Insets from images A3 and A6 are magnified in B3 and B6 respectively, in order to illustrate some vesicles. In C3 and C6, the brightness and contrast of these insets were modified in order to enhance visualization of the AuNPs contained in the vesicles. The sequential images in the stack allowed us to reconstruct in 3D structures such as the basal membrane or the vesicles located inside the BCEC, by manually tracing the area in consecutive planes. However, this strategy cannot be used with AuNPs, because they are located in one or another section, but never in more than one section, so it is impossible to reconstruct these particles in 3D by manually tracing the area across consecutive planes. Thus, a copy of the stack was preprocessed using the Fiji software in order to later replace the AuNPs in each section by 3D spheres of similar size (20 nm diameter) in Imaris. Since the AuNPs are the darkest structures in these images, they could be segmented with the Fiji software using a low threshold value. An example of the AuNPs segmentation can be observed in Figure 4, images D3 and D6, which correspond to the regions shown in B3 and B6 respectively. It must be pointed that in some individual cases, the darkness of the vesicle hinders visualization of the AuNPs, and thus some AuNPs may be missing from the 3D reconstruction. After segmentation, the resulting binary particles were split using a watershed to allow individual reconstruction. The final binary stack of images was loaded into Imaris as an additional channel of the original stack and the AuNPs

were rendered as spheres in the final 3D reconstruction. Thus, this level of magnification and this strategy allowed for reliable 3D reconstructions in which the structures of the BBB, such as the BCECs, their basal membrane, and the vesicles located in the BCECs, as well as the precise location of the AuNPs could be visualized simultaneously. To facilitate the visualization of the vesicles and the AuNPs, we previously removed the region corresponding to the lumen using the Fiji software. Representative images of the 3D reconstruction from the SBF-SEM high-magnification image stack that contains sections A1-A6 can be observed in Figure 4, images E1 and F1. An animation of this reconstruction can be observed in Online Resource 5. In the reconstructions performed at high-level magnification, we observed that all AuNPs found (we found a total of 96 AuNPs in the different samples analyzed) were located inside endocytic vesicles in the BCECs. No AuNPs were found on the luminal side of the BCEC or in the basal membrane of the endothelium. Regarding the distribution of the AuNPs inside the vesicles, in some cases they were randomly distributed (Fig 4, image E2), while in others they appeared in the marginal region of the vesicle, near the membrane (Figure 4, image F2). With respect to the shape of the vesicles, the 3D reconstruction allowed us to observe that although some of the vesicles containing 8D3–AuNP conjugates present a spherical or ellipsoidal form, they are often branched structures with irregular shapes, which sometimes even seem to merge with each other forming a complex endosomal network. As can be observed in Figure 4, some vesicles that show a spherical or ellipsoidal shape in a 2D plane can be considered part of a complex and irregular structure when subsequent sections are analyzed as a whole 3D structure.

DISCUSSION

As stated above, our first goal in this work was to establish and optimize the imaging conditions and configuration settings of the SBF-SEM to apply this technique to BBB sections, and to study the transport of AuNPs coated with an anti-TfR mAb.

The main problem with the use of this technique for our application was the charging of the samples. In order to decrease this charging, we used intensive osmium reactions

and *en bloc* staining with heavy metals before embedding the samples, as well as sputter coating. However, the presence of bare resin in the lumen of the capillaries, the need for higher-magnification images, the use of higher voltages and the longer dwell times used to enhance both the signal-to-noise ratio and visualization of the AuNPs, caused charging and damage to the samples, hampering the serial imaging process. These observations are in agreement with previous work (Nguyen et al. 2016; Ohno et al. 2015) and currently, efforts are being made to overcome this problem, which is particularly prominent in SBF-SEM imaging. Nguyen et al. showed that increasing conductivity by using carbon-based conductive resins significantly reduces the charging of the samples during SBF-SEM imaging, and improves the resolution of the images by facilitating their cutting (Nguyen et al. 2016).

Meanwhile, the small size of the AuNPs (20 nm) was the major limiting factor as well as the key challenge when trying to visualize and render the particles in 3D. Low-magnification imaging was relatively easy, as the lower resolution of the images required a lower accelerating voltage, and thus there was less charging in tissue. As shown in Figures 2 and 3, this level of magnification permits acquiring images of a large field of view and monitoring of relatively long capillary segments (more than 10 μm long), and results appropriate for the identification and 3D reconstruction of cellular elements and some subcellular elements as nuclei. However, this resolution was too low for clear identification of the AuNPs. This led us to increase the level of magnification and re-establish the setting parameters. A higher accelerating voltage permitted high-magnification image acquisition with sufficient resolution for AuNP visualization, as exemplified in Figure 4. These conditions dramatically increased the charging of the tissue, but permitted us to acquire serial images (a maximum of 50 images in each stack) that are sufficient to study the AuNPs trafficking.

Thus, adjusting the balance among the different variables listed above (voltage, level of magnification, dwell time, chamber pressure and image size) and working under very specific conditions (as detailed in the Results section), allowed us to overcome this charging problem. We thus achieved the goal of reconstructing BBB segments and vesicles containing AuNPs in 3D, as well as precisely localizing the AuNPs within the

cellular structures. As it was impossible to reconstruct the AuNPs in 3D by manually tracing the area in consecutive planes, we applied an innovative method in which we replaced the AuNPs by 3D spheres of a similar size at the exact same coordinates inside the tissue volume. In this way, we were able to visualize the AuNPs as 3D spheres inside the 3D tissue reconstructions.

A further consideration is that although theoretically the in-chamber ultramicrotome can cut sections as thin as 20-30 nm, we found that due to the presence of bare resin in the lumen of the capillaries and the ensuing charging, it was impossible to cut sections thinner than 70 nm. Consequently, information was lost when parts of the sample that did not contribute to the image were cut away. This led us to address that some information was lost along the z-axis. Although this loss of information does not seem to influence the rendering of subcellular elements such as the vesicles, it may affect the visualization of some AuNPs. We therefore need to bear in mind that there might be more AuNPs than those observed. There is an alternative SEM-based volume imaging method, in which tissue can be removed by milling the sample surface with a focused ion beam (FIB) (Briggman and Bock 2012; Kremer et al. 2015). Both methods are based on the principle of block-face imaging, in which the surface of a plastic embedded block of cells or tissue is imaged and then sectioned and reimaged (Kremer et al. 2015). However, the FIB-SEM technique offers a higher z-resolution of 5 nm and allows imaging at the isotropic voxel (Briggman and Bock 2012; Kremer et al. 2015). This technique is probably best suited for AuNP localization and 3D rendering, as it currently provides the highest 3D resolution, but it is limited to small volumes, whereas SBF-SEM can handle much larger volumes. Moreover, ion beam milling is much slower than sectioning with a diamond-knife, and the need for milling consistency also restricts the available field of view (to as little as 20 μm^2) (Peddie and Collinson 2014). As discussed by Briggman and Bock, there is currently no one best volume EM imaging method (Briggman and Bock 2012): each method involves tradeoffs in size, resolution and completeness. Thus, a combination of both techniques would be the best choice, as they can complement each other. In any case, we can conclude that, although we probably did not visualize all the AuNPs during the process,

the techniques and strategies used in the present work provide information on the transport or trafficking of AuNPs coated with an anti-TfR mAb on the BBB.

After obtaining the high-magnification images, the subsequent 3D analysis of the vesicles containing AuNPs yielded considerable information on the size and shape of these vesicles and the organization of the endosomal network inside BCECs. It also allowed us to complement our previous 2D TEM studies with regard to how AuNPs coated with the anti-TfR 8D3 antibody are processed in BCECs (Cabezón et al. 2015).

In our previous work, we postulated that vesicles that contain AuNPs were generally spherical or ellipsoidal vesicles of different sizes. However, the passage from 2D to 3D has revealed that these vesicles, at least those that contain a high number of AuNPs, are not large spherical or ellipsoidal vesicles but complex vesicular networks of up to 1 μm in size, and maybe even larger. So we can now assume that many of the supposedly spherical or ellipsoidal vesicles we analyzed in a 2D plane are in fact part of these complex networks; thus, the number of AuNPs per vesicle may be significantly higher than we concluded in our previous 2D study. In the present study, we administered the AuNPs coated with 8D3 intravenously and analyzed vesicles in BCECs by killing the animals 2.5 h after the intravenous administration. The fact that we observed high numbers of AuNPs in the complex networks suggests that endosomal sorting occurs relatively quickly. In our previous 2D study, and after 2.5 h of recirculation, 95% of the AuNPs were observed inside endocytic vesicles of the BCECs; 4.6% of the AuNPs were located in the basal membrane of the endothelium, attached to the abluminal membrane of the BCEC; and just 0.2% of AuNPs were found located in the lumen of the capillary, attached to the luminal membrane of the cell or being internalized via clathrin-coated pits. In the present work, all the AuNPs were found inside endocytic vesicles, in agreement with the most frequent localization pattern observed in the previous study. In any case, pooling the information obtained from both the present and the previous study, we can conclude that AuNPs individually internalize inside BCECs via clathrin-dependent endocytosis. In the main route, the resulting endocytic vesicles fuse with early endosomes and enter the endosomal network, where vesicular fusion, maturation, sorting and rearrangement occur. It must

be pointed that, in the case of the endosomal route of transferrin internalized via TfR, the resulting sorting endosomes may become acidified by ATP-dependent proton-pumps before their maturation into late endosomes. With this acidification, some receptors (TfR) and ligands (transferrin) dissociate and are recycled for another round of delivery (Hillarieau and Couvreur 2009). This pattern matches the AuNP localization observed in our previous 2D study. There, some of the AuNPs were observed attached to the vesicle membrane, whereas others seemed to be dissociated from the membrane, and possibly from the TfR. In the present 3D study, we observed similar patterns: while in some cases the AuNPs are randomly distributed inside the vesicle, in some others they seem to be in a peripheral disposition and thus probably attached to the vesicle membrane. In any case, in this route, the AuNPs end up accumulated in these complex vesicular networks, whose nature remains to be clarified.

Observing the vesicular network (Figure 4, images E1 and F1), it can be seen that AuNPs accumulate in certain regions, whereas extended areas in other regions of the vesicular network are completely free of AuNPs. The presence of clusters of AuNPs inside the vesicular network may reflect the localization of the subdomains of the complex network, which could be useful to describe the trafficking of the AuNPs. In order to identify and characterize the different subdomains of the vesicular networks, utilization of SBF-SEM together with TEM (conventional or combined with immunostaining) would be a promising strategy, worthy of consideration in future studies. Moreover, it would be interesting to study earlier and later time points than the 2.5 h used in the present study, such as the 10 min or 24 h time points analyzed in our previous 2D study. In any case, although most of the vesicles follow this main route, in our previous 2D study we observed that some AuNPs reached the basal lamina of the endothelium, remaining attached to the basolateral membrane of the BCEC. In the present study no AuNPs were found in the basal membrane of the capillaries, probably due to the small number of them that complete transcytosis and the limited number of capillary images that we have been able to analyze in this study. Be that as it may, in the previous study we observed no AuNPs far away from the basal membrane, i.e., in the brain parenchyma.

In summary, SBF-SEM imaging and 3D reconstruction of vesicles containing AuNPs provide complementary information on their morphology and reinforce the 8D3-AuNP trafficking model proposed in our previous study. Combining this technique with other volume EM imaging techniques is worth of considering for studies of drug transport across the BBB. The attachment of AuNPs to drugs or carriers could be a good strategy to monitor these substances in the most precise and accurate manner currently available.

ACKNOWLEDGEMENTS

FIGURE CAPTIONS

Fig. 1 Deduced trafficking of 8D3-AuNPs across the mouse BBB (from Cabezón et al., 2015). The 8D3–AuNPs internalize individually within BCECs via TfR-mediated and clathrin-dependent process. These vesicles then follow at least two different routes. On one hand, most vesicles enter intracellular processes of vesicular fusion and rearrangement in which the AuNPs end up accumulated inside vesicles with a high AuNPs content. On the other hand, a small percentage of the vesicles follow a different route in which they fuse with the abluminal membrane and open to the basal membrane. In these cases, the 8D3–AuNPs remain attached to the abluminal membrane, which suggests an endosomal escape, but not dissociation from the TfR.

Fig. 2 (A1-C1) Three selected serial images from an SBF-SEM low-magnification image stack. The complete sequence of images can be visualized in Online Resource 1. (A2-C2) Colored areas represent some of the structures that were selected and manually traced in A1-C1 respectively, for the later 3D reconstruction. The selection process was performed on all the serial images in the stack. The resulting 3D reconstruction of the capillary segment containing the different cellular elements that form the neurovascular unit can be observed in the video contained in Online Resource 3. (D1-D3) Three snapshots of the Online Resource 3 video showing the 3D reconstruction: (D1) Two adjacent endothelial cells (ec1 and ec2) can be observed. Image B1 is superimposed on the reconstruction. (D2) A pericyte rendering is added to the reconstruction. (D3) The complete 3D reconstruction of the BBB segment, which includes the renderings of the two adjacent endothelial cells, the pericyte and two astrocytic endfeet (ae1 and ae2). Abbreviations: ec, endothelial cell; p, pericyte; ae, astrocytic endfeet. Scale bar: 5 µm

Fig. 3 (A1-C1) Three selected serial images from an SBF-SEM low-magnification image stack. The complete sequence of images can be visualized in Online Resource 2. (A2-C2) Colored areas represent the structures that were selected and manually traced in A1-C1 respectively, for later 3D reconstruction: an endothelial cell, a pericyte and their respective nuclei. The selection process was performed on all the serial images in the stack. The resulting 3D reconstruction can be observed in the video contained in Online Resource 4. (D1-D2) Two snapshots of the video showing the 3D reconstruction. In D1, part of the tissue volume is represented to contextualize the 3D reconstruction of the capillary segment. Abbreviations: ec, endothelial cell; n1, endothelial cell nucleus; p, pericyte; n2, pericyte nucleus; bm, basal membrane. Scale bar: 5 µm

Fig. 4 (A1-A6) Six selected serial images from an SBF-SEM high-magnification image stack. Arrows indicate vesicles containing AuNPs. (B3 and B6) Original insets from A3 and A6, respectively. (C3 and C6) Insets from A3 and A6, respectively, in which the brightness and contrast has been modified in order to enhance visualization of the AuNPs. (D3 and D6) Images corresponding respectively to the insets from A3 and A6 that were obtained after applying the process of binarization, which permits us to localize the AuNPs. (E1 and F1) Representative images of the 3D reconstruction of the SBF-SEM high-magnification image stack that contains images A1-A6. AuNPs are represented as green spheres. Blue regions are the endothelial vesicles. bm: basal membrane; lum: lumen of the capillary. An animation of this reconstruction can be observed in Online Resource 5. (E2 and F2) Insets from E1 and F1, respectively. The arrow in E2 indicates AuNPs that are irregularly distributed inside the vesicle, while the arrow in F2 indicates AuNPs with a peripheral distribution. Scale bar: 2 μm

ONLINE RESOURCE CAPTIONS

Online Resource 1 Serial images from an SBF-SEM low-magnification image stack. The magnification is 14,900 x and the voxel size 16 x 16 x 100 nm

Online Resource 2 Serial images from an SBF-SEM low-magnification image stack. The magnification is 11,130 x and the voxel size 22.1 x 22.1 x 70 nm

Online Resource 3 Video illustrating, from different perspectives, two adjacent BCECs (different shades of red), a pericyte (blue) and two different astrocytic endfeet (different shades of green) rendered after processing the images from the stack shown in Online Resource 1

Online Resource 4 Video illustrating, from different perspectives, a BCEC (red) and a pericyte (blue) and their respective nuclei (bright red an bright blue, respectively), rendered after processing the images from the stack shown in Online Resource 2

Online Resource 5 Video illustrating, from different perspectives, the basal membrane (yellow), the vesicles in the BCEC (blue) and the AuNPs contained in those vesicles (green spheres). The SBF-SEM high-magnification images of the stack were obtained at 35,850 x magnification and the voxel size is 4.8 x 4.8 x 100 nm

REFERENCES

Abbott N J, Patabendige A A K, Dolman D E M, Yusof S R, Begley D J (2010) Structure and function of the blood-brain barrier. Neurobiol Dis 36: 437-449

Alata W, Paris-Robidas S, Emond V, Bourasset F, Calon F (2014) Brain uptake of a fluorescent vector targeting the transferrin receptor: a novel application of in situ brain perfusion. Mol Pharmaceutics 11: 243-253

Briggman K L, Bock D D (2012) Volume electron microscopy for neuronal circuit reconstruction. Curr Opin Neurobiol 22: 154-161

Cabezón I, Manich G, Martín-Venegas R, Camins A, Pelegrí C, Vilaplana J (2015) Trafficking of gold nanoparticles coated with the 8D3 anti-transferrin receptor antibody at the mouse blood-brain barrier. Mol Pharmaceutics 12: 4137-4145

de Boer A G, Gaillard P J (2007) Drug targeting to the brain. Annu Rev Pharmacol Toxicol 47: 323-355

Deerinck T J, Bushong E, Thor A, Ellisman M H (2010) NCMIR methods for 3D EM: A new protocol for preparation of biological specimens for serial block face scanning electron microscopy. Microscopy pp 6-8

Freskgård P O, Urich E (2016) Antibody therapies in CNS diseases. Neuropharmacology. doi: 10.1016/j.neuropharm.2016.03.014

Gosk S, Vermehren C, Storm G, Moss T (2004) Targeting antitransferrin receptor antibody (OX26) and OX26-conjugated liposomes to brain capillary endothelial cells in situ perfusion. J Cereb Blood Flow Metab 24: 1193-1204

Hillaireau H, Couvreur P (2009) Nanocarriers' entry into the cell. Cell Mol Life Sci 66: 2873–2896

Kremer A, Lippens S, Bartunkova S et al (2015) Developing 3D SEM in a broad biological context. J Microsc 259: 80-96

Lajoie J M, Shusta E V (2015) Targeting receptor-mediated transport for delivery of biologics across the blood-brain barrier. Annu Rev Pharmacol Toxicol 55: 613-631

Lee H J, Engelhardt B, Lesley J, Bickel U, Pardridge W M (2000) Targeting rat anti-mouse transferrin receptor monoclonal antibodies through blood-brain barrier in mouse. J Pharmacol Exp Ther 292: 1048-1052

Manich G, Cabezón I, Del Valle J, Duran-Vilaregut J, Camins A, Pallàs M, Pelegrí C, Vilaplana J (2013) Study of the transcytosis of an anti-transferrin receptor antibody with a Fab' cargo across the blood-brain barrier in mice. Eur J Pharm Sci 49: 556-564

Moos T, Morgan E H (2001) Restricted transport of anti-transferrin receptor antibody (OX26) through the blood-brain barrier in the rat. J Neurochem 79: 119-129

Nguyen H B, Thai T Q, Saitoh S, Wu B, Saitoh Y, Shimo S, Fujitani H, Otobe H, Ohno N (2016) Conductive resins improve charging and resolution of acquired images in electron microscopic volume imaging. Sci Rep. doi: 10.1038/srep23721

Ohno N, Katoh M, Saitoh Y, Saitoh S, Ohno S (2015) Three-dimensional volume imaging with electron microscopy toward connectome. Microscopy 64: 17-26

Pardridge W M (1998) CNS drug design based on the principles of blood-brain barrier transport. J Neurochem 70: 1781-1792

Paris-Robidas S, Emond V, Tremblay C, Soulet D, Calon F (2011) In vivo labeling of brain capillary endothelial cells after intravenous injection of monoclonal antibodies targeting the transferrin receptor. Mol Pharmacol 80: 32-39

Peddie C J, Collinson L M (2014) Exploring the third dimension: Volume electron microscopy comes of age. Micron 61: 9-19

Schindelin J, Arganda-Carreras I, Frise E et al (2012) Fiji: an open-source platform for biological-image analysis. Nat Methods 9: 676-682

Temsamani J, Rousselle C, Rees A R, Scherrmann J M (2001) Vector-mediated drug delivery to the brain. Expert Opin Biol Ther 1: 773-782

Zhang Y, Calon F, Zhu C, Boado R J, Pardridge W M (2003) Intravenous nonviral gene therapy causes normalization of striatal tyrosine hydroxylase and reversal of motor impairment in experimental parkinsonism. Hum Gene Ther 14: 1-12

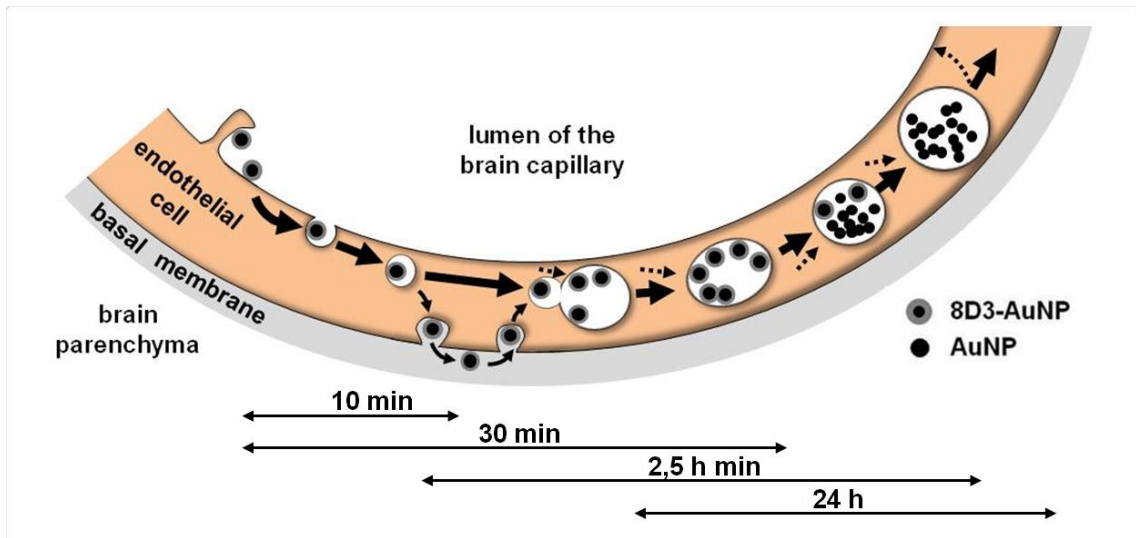Zhang Y, Pardridge W M (2005) Delivery of β-galactosidase to mouse brain via the blood-brain barrier transferrin receptor. J Pharmacol Exp Ther 313: 1075-1081
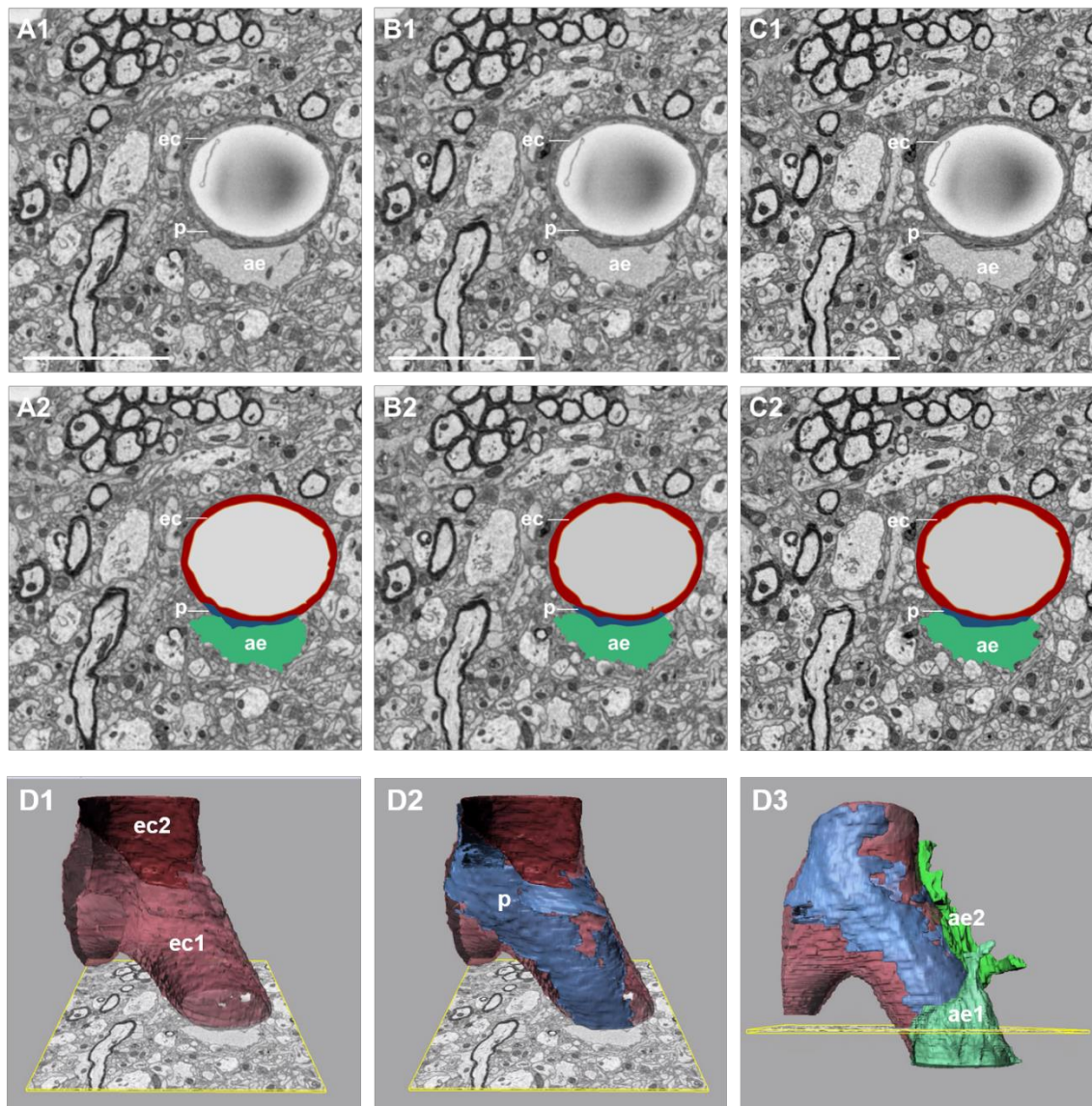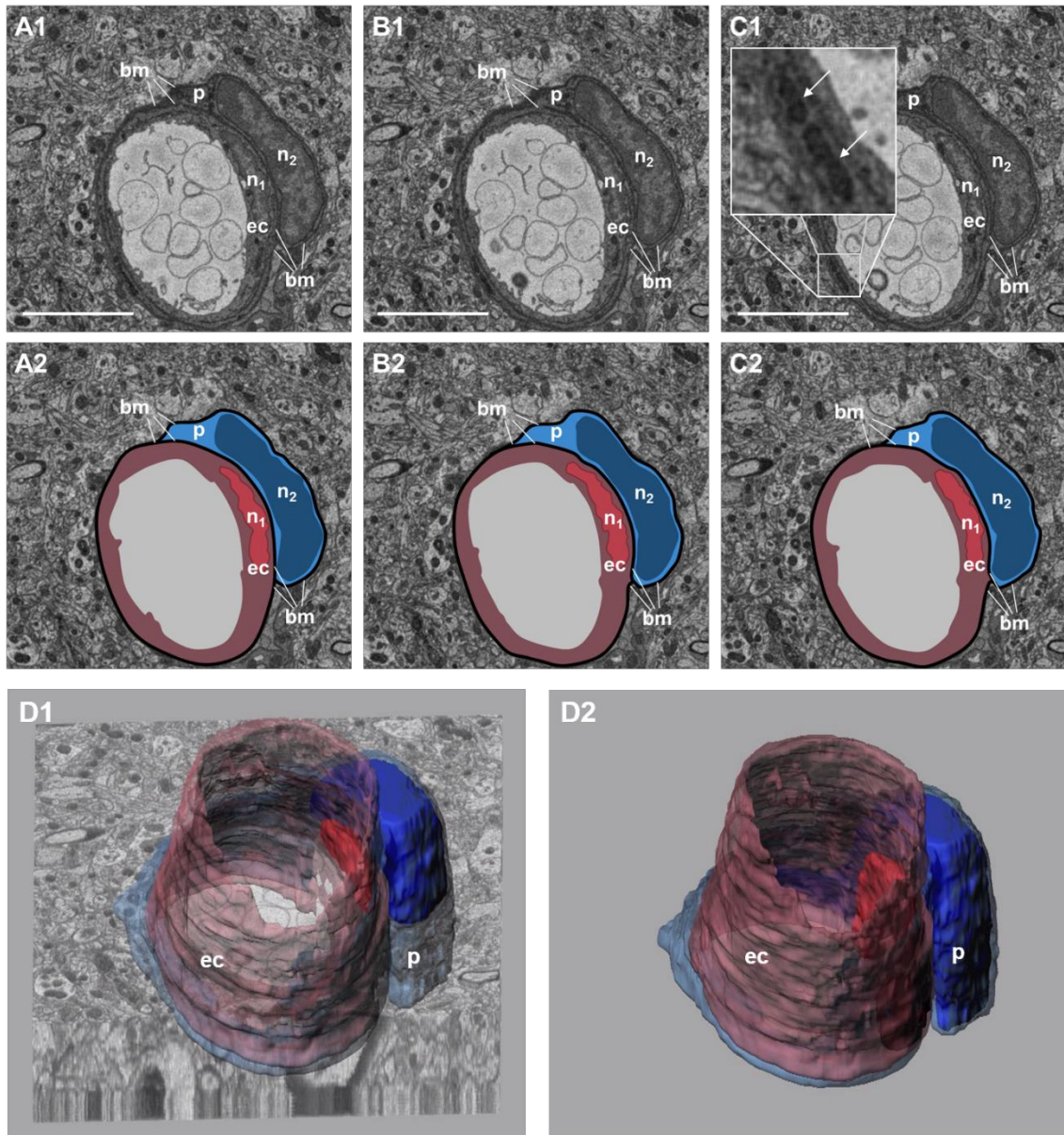
Figure 1

Figure 2

Figure 3

Figure 4